IEEE Access
Multidisciplinary | Rapid Review | Open Access Journal

Received November 28, 2019, accepted January 23, 2020, date of publication February 3, 2020, date of current version February 11, 2020.

Digital Object Identifier 10.1109/ACCESS.2020.2971423

Nonlinear Regression Color Correction Method for RGBN Cameras

ZHENGHAO HAN[1], WEIQI JIN[1], LI LI[1], XIA WANG[1], XIAOFENG BAI[2], AND HAILIN WANG[1]

[1]Key Laboratory of Photo-Electronic Imaging Technology and Systems, School of Optics and Photonics, Ministry of Education of China, Beijing Institute of Technology, Beijing 100081, China
[2]Science and Technology on Low-Light-Level Night Vision Laboratory, Xi'an 710065, China

Corresponding author: Weiqi Jin (jinwq@ bit.edu.cn)

This work was supported in part by the Pre-study Foundation of the Army Armament Department of China under Grant 6140414050327, and in part by the Foundation of Science and Technology at the L3 Night Vision Laboratory J20170101.

ABSTRACT With the development of multi-spectral imaging techniques, many new multi-spectral imaging devices have been developed in recent years. Red-green-blue and near-infrared (RGBN) cameras are widely used because they capture visible light and near-infrared light simultaneously, but they inevitably introduce color desaturation. Because there is clear multicollinearity among the RGBN channels, the ordinary least squares regression (OLSR) color correction method performs poorly. To solve color bias and multicollinearity, an RGBN camera color correction pipeline is proposed. A large number of nonlinear regression color correction methods that consist of combinations of four regression methods and nine nonlinear transforms are evaluated in this study. The results show that the proposed OLSR-based compound transform color correction method and partial least-squares regression (PLSR) based Gaussian-core transform color correction method yield better color correction results and are more robust. These approaches reduce the multicollinearity of the RGBN camera channels and will be a valuable reference in the development of RGBN imaging applications.

INDEX TERMS Color correction, multicollinearity near-infrared, nonlinear regression, RGBN camera.

I. INTRODUCTION

Color imaging and multi-spectral imaging techniques are widely used in fields such as environmental observation [1], defense and security [1], biomedical applications [1], agriculture [2], product quality assessment [2], material classification [2] and night vision [3]. Siliconbased sensors can capture multi-spectral information through a color filter array (CFA) coating placed in front of the sensor. Furthermore, if the sensor's relative spectral sensitivity which is calculated using the sensor's spectral sensitivity and the CFA's spectral transmittance is consistent with the distribution of a standard observer's tristimulus, this enables us to obtain color images that is close to human vision.

Most current color digital cameras use the well-known Bayer CFA, and the camera's spectral sensitivity is limited to visible light. The signal-to-noise-ratio (SNR) of these cameras decreases rapidly as the intensity of the environmental illumination decreases. Generally speaking, the minimum working environmental illumination of a camera is 10^{-1} lx or 5×10^{-2} lx. Although we could further decrease this value to 5×10^{3} lx by enlarging the pixel size of the sensor (at the expense of resolution), the loss outweighs the gain. To enable both color vision in the daylight and invisible-light color night vision, RGBN CFAs replace one green channel of the Bayer CFA with a near-infrared (NIR) channel and extend the spectral transmittance of the color filter to NIR light, as shown in Figure 1. A NIR cut-off filter (IRCF) is used to block NIR light to achieve correct color vision in the daylight, and the IRCF is removed at night so that the camera can sense the additional NIR illuminant. It was found that color images captured with color filters with the extended spectral transmittance have a better SNR, but introduce severe color bias and desaturation. As a result, RGBN camera color restoration methods with IRCF removal have been proposed. These methods enable RGBN cameras improve color vision while retaining a good SNR.

The relative spectral sensitivity of an RGBN camera is not consistent with the distribution of a standard observer's tristimulus, and the environment illumination always differs

The associate editor coordinating the review of this manuscript and approving it for publication was Jeon Gwanggil.

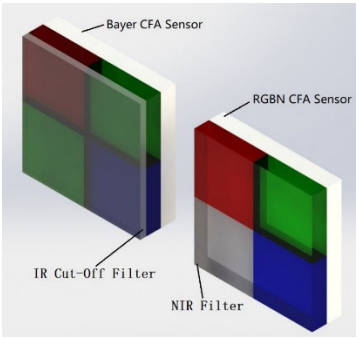

FIGURE 1. RGBN camera CFA arrangement.

from a standard illuminant, so it is necessary to restore the colors of RGBN camera images. RGBN camera color correction methods can be divided into color correction matrix (CCM) based methods, spectral decomposition based methods, sensor spectral sensitivity curve optimization based methods, and learning based methods.

Park et al. [4] improved the traditional 3×4 CCM method by introducing RN, GN, and BN constraints. The nature of Park et al.'s method is to introduce a nonlinear constraint for RGBN channels, but this constraint is too simple to substantially improve color correction accuracy. Chen et al. [1] proposed a 3×19 CCM by introducing R2, G2, B2, RB, RB, GB, R3, G3, B3, R2G, R2B, G2B, G2R, G2B, B2R, and B2G constraints. In detail, this method incorporates a new cubic polynomial constraint with a zero coefficient high-order N term. Using a quasi-linearization technique, it calculates the CCM using ordinary least squares regression (OLSR). Increasing the order of the polynomials increases the risk of overfitting, in which case the generalization ability of the model is not guaranteed. Monno et al. [5] use the chromatic values of color checker patches as samples to calculate the CCM through OLSR and investigate polynomial and root polynomial transforms. Teranaka et al. [6] took demosaicing, CFA arrangement, and color restoration into consideration, using a 3×4 CCM for color correction.

Park et al. [7], Kwon et al. [8], and Park et al. [9] developed a spectral decomposition based method that decomposes the NIR band into a color-correlated NIR band and color-independent NIR band to obtain each element of a 3×4 CCM. However, this method still relies on linear regression. The 3×4 CCM calculated by OLSR is the optimal unbiased estimation of the corrected color, and any modification decreases the color correction accuracy. Hertel et al. [10] optimized traditional 3×4 CCM by calculating the differences of sensor's relative spectral sensitivity curve and a destination relative spectral sensitivity curve. The color correction accuracy still cannot surpass that of an OLSR-based 3×4 CCM. Yamashita et al. [3] separately calculate the integration of the NIR band sensitivity curve and the NIR part of the visible band sensitivity curve to obtain a constant ratio. They corrected the colors by then directly subtracting the visible band and the constant ratio of the NIR band, proposing two

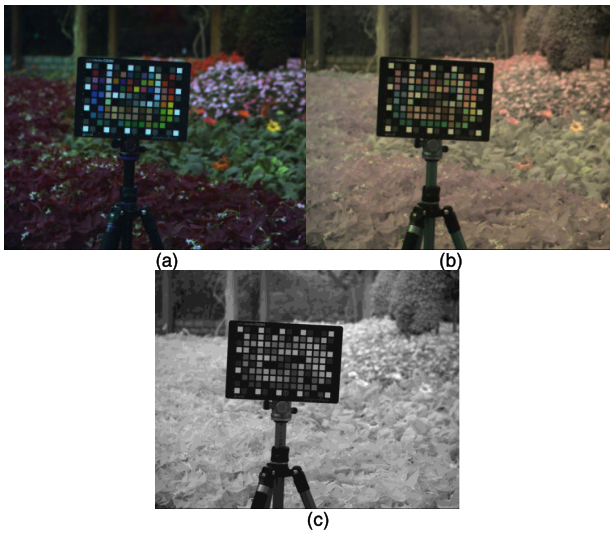

FIGURE 2. Image color desaturation when NIR light is introduced. (a) image captured with an IRCF, (b) image captured without an IRCF, and (c) NIR image.

optimized versions in the same year [11], [12]. Zahra et al. [2] optimized the traditional 3×4 CCM by calculating the differences in the sensor's relative spectral sensitivity curve and a designed ideal relative spectral sensitivity curve. The core of these methods is still OLSR. Without introducing nonlinear constrains, these approaches cannot surpass an OLSR-based 3×4 CCM color correction method.

Aguilera et al. [13] proposed a neural network based RGBN camera color correction method using a simple net structure. They use only two fully-connected-layers between the input layer and output layer. Subsequently, Soria *et al.* [14] used different optimizers and activation functions with another simple network structure to correct colors. They later trained the model with a convolutional neural network [15].

Most Bayer CFA based industrial cameras, commercial digital cameras, and smartphones correct colors using an OLSR method. A set of CCMs are calibrated under different illuminations and one is chosen for color correction during use. This widely accepted color correction method obtains satisfactory results. However, in RGBN camera color-correction applications, although OLSR-based color-correction approaches yield good results for indoor scenes with weak NIR light, color bias occurs in corrected outdoor scenes because of the strong NIR-light reflection of plants, as shown in Figure 2. Moreover, RGBN channels are strongly correlated. Hence, calculating CCM using OLSR may lead to severe round-off errors, which can directly cause poor color correction results. To improve the accuracy and robustness of RGBN camera color correction, suitable nonlinear transforms and regression methods should be investigated.

Hence, this study investigates nine nonlinear transform models and four regression methods: OLSR, ridge least squares regression (RLSR), principal components

regression (PCR), and partial least squares regression (PLSR). By comparing all 40 potential color correction methods (4 regression methods × 10 transformations including 9 nonlinear transform), we determine the best-performing color correction method.

II. RGBN CAMERA COLOR CORRECTION METHOD

A. RGBN CAMERA COLOR CORRECTION MODEL

1) NECESSITY OF NONLINEAR REGRESSION

Most industrial cameras, commercial digital cameras and smartphones would place an IRCF in front of each sensor and use the chromatic values of color checker patches and calculate the CCM using OLSR. For normal visible scene applications, the results of this color correction method are satisfactory. In contrast, for an RGBN camera, the IRCF is removed. Hence, there is a more complicated mapping relationship between real colors and image colors. In addition, we cannot obtain satisfactory color correction results through simple linear regression. Nonlinear transforms must hence be introduced.

RGBN camera imaging is more complicated than normal visible camera imaging from the point of view of its model. The image of a target scene captured by an RGBN camera is denoted as a matrix $P_{n\times 4}$, where n represents the RGBN camera's total pixel count. Each column of P is a color channel pixel array, i.e., $P_{n\times 4} = [R_{n\times 1}, G_{n\times 1}, B_{n\times 1}, N_{n\times 1}]$. Let $P(:, i)$ denote the ith column of P. Then [16],

$$\mathrm{P}(:, i) = \alpha \cdot \int_{380}^{1100} I(\lambda) \cdot R(\lambda) \cdot S(\lambda) \cdot F_i(\lambda) d\lambda + \varepsilon \quad (1)$$

Here, $I(\lambda)$ represents the spectral power distribution function of the illumination, $R(\lambda)$ represents the spectral reflectivity function of the scene with respect to pixel location, $\mathrm{S}(\lambda)$ represents the spectral response function of the sensor, and $F_i(\lambda)$ represents the ith channel filter's spectral transmittance function. Further, α represents the linear coefficient and ε represents the image noise at each pixel location.

In this study, images captured by an RGBN camera with an IRCF are treated as ground truth images. Let $Q_{n\times 3}$ be the ground truth image matrix, i.e., $Q_{n\times 3} = [GTR_{n\times 1}, GTG_{n\times 1}, \mathrm{GT}B_{n\times 1}]$. Then,

$$\mathrm{Q}(:, i) = \alpha_0 \cdot \int_{380}^{760} I(\lambda) \cdot \mathrm{R}(\lambda) \cdot \mathrm{S}(\lambda) \cdot \mathrm{F}_{0i}(\lambda) d\lambda + \varepsilon_0 \quad (2)$$

The difference between $\mathrm{F}_{0i}(\lambda)$ and $\mathrm{F}_i(\lambda)$ is that NIR light can pass through $\mathrm{F}_i(\lambda)$ but not $\mathrm{F}_{0i}(\lambda)$.

Because they go through the same imaging process, P and Q have the same form. The only differences are the upper limit of integral and the spectral transmittance functions of the filters. Suppose

$$Q(:, i) = P(:, i) + f(\lambda) \quad (3)$$

Then, $f(\lambda)$ has the form

$$\begin{aligned} f(\lambda) &= \beta \cdot \int_{380}^{760} I(\lambda) \cdot \mathrm{R}(\lambda) \cdot \mathrm{S}(\lambda) \cdot \Delta \mathrm{F}_i(\lambda) d\lambda \\ &\quad + \gamma \cdot \int_{760}^{1100} I(\lambda) \cdot \mathrm{R}(\lambda) \cdot \mathrm{S}(\lambda) \cdot \Delta \mathrm{F}_i(\lambda) d\lambda + \xi \\ &= \beta \cdot h(\lambda) + \gamma \cdot g(\lambda) + \xi \end{aligned} \quad (4)$$

where $\Delta F_i(\lambda) = F_i(\lambda) - F_{0i}(\lambda)$.

Generally speaking, the chromatic values of color checker patches are utilized to calculate the CCM for RGBN camera color correction. The nature of this procedure is to fit $f(\lambda)$ with limited data. We only know $\mathrm{S}(\lambda)$ and $\Delta F_i(\lambda)$, and they are not accurate. $I(\lambda)$ is often supposed to be one of a few limited types, and $R(\lambda)$ is remains an arbitrary unknown function. Hence, the optimal $f(\lambda)$ cannot be calculated theoretically. As a result, RGBN camera color correction is different from normal commercial visible camera color correction. For normal visible cameras, the form of $f_{\mathrm{Vis}}(\lambda)$ is

$$\begin{aligned} f_{Vis}(\lambda) &= \beta \cdot \int_{380}^{760} I(\lambda) \cdot \mathrm{R}(\lambda) \cdot \mathrm{S}(\lambda) \cdot \mathrm{F}_i(\lambda) d\lambda + \xi \\ &= \beta \cdot h_{Vis}(\lambda) + \xi \end{aligned} \quad (5)$$

Function $f(\lambda)$ has a form that is more complicated than that of $f_{\mathrm{Vis}}(\lambda)$ and is best represented using nonlinear transforms.

2) NONLINEAR REGRESSION MODEL

As described above, the nonlinear transform of an image P captured by an RGBN camera and the ground truth image Q is arbitrary and unknown for various scenes. When the relationships between independent and dependent variables are unknown, typical nonlinear functions are usually used to fit the function. Then, the best performing nonlinear estimation is chosen using proper evaluation indices.

The nonlinear transform models evaluated in this study all can be quasi-linearized and estimated by common regression methods. They are shown in Table 1. Let R_0, G_0, and B_0 be the corrected color channels, and let R, G, B, and N be the input image channels with color bias. In an RGBN camera color-correction model, there are three dependent variables and four independent variables. To simplify the notation, the nonlinear transforms are written with one dependent variable and two independent variables. Hence, y denotes the dependent variable of a nonlinear transform function and x_1 and x_2 denote the independent variables.

3) QUASI-LINEARIZATION IN NONLINEAR REGRESSION

Linear regression methods are widely used in model parameter estimation applications and are easy to calculate. However, the model must be linear and of the following form:

$$y = \alpha_0 + \alpha_1 \cdot x_1 + \alpha_2 \cdot x_2 + \ldots + \alpha_p \cdot x_p \quad (6)$$

Quasi-linearization enables nonlinear transform model parameter prediction to be calculated using linear regression. This kind of nonlinear model has the following

TABLE 1. Nonlinear transform models.

Model Name		Form of the Model Function
Polynomial	Transform function	$\mathrm{y}=\alpha+\beta_1\cdot x_1+\beta_2\cdot x_2+\beta_3\cdot x_1^2+\beta_4\cdot x_2^2+\beta_5\cdot x_1\cdot x_2$
	Quasi-linearized form	$[\mathrm{R}_0\ G_0\ B_0]^T=CCM\cdot[\mathrm{R\ G\ B\ N}\ R^2\ G^2\ B^2\ N^2\ \mathrm{RG\ RB\ RN\ GB}\ G\ \mathrm{N\ BN\ 1}]^T$
Root Polynomial	Transform function	$\mathrm{y}=\alpha+\beta_1\cdot x_1+\beta_2\cdot x_2+\beta_5\cdot\sqrt{x_1\cdot x_2}$
	Quasi-linearized form	$[\mathrm{R}_0\ G_0\ B_0]^T=CCM\cdot[\mathrm{R\ G\ B\ N}\ \sqrt{RG}\ \sqrt{RB}\ \sqrt{RN}\ \sqrt{GB}\ \sqrt{GN}\ \sqrt{BN}\ 1]^T$
Logarithm	Transform function	$\mathrm{y}=\alpha+\beta_1\cdot\ln x_1+\beta_2\cdot\ln x_2$
	Quasi-linearized form	$[\mathrm{R}_0\ G_0\ B_0]^T=CCM\cdot[\mathrm{lnR\ ln}G\ \mathrm{ln}B\ \mathrm{ln}N\ 1]^T$
Inverse	Transform function	$\mathrm{y}=\alpha+\frac{\beta_1}{x_1}+\frac{\beta_2}{x_2}$
	Quasi-linearized form	$[\mathrm{R}_0\ G_0\ B_0]^T=CCM\cdot\left[\frac{1}{R}\ \frac{1}{G}\ \frac{1}{B}\ \frac{1}{N}\ 1\right]^T$
Power	Transform function	$\mathrm{y}=\alpha\cdot x_1^{\beta_1}\cdot x_2^{\beta_2}$
	Quasi-linearized form	$[\mathrm{lnR}_0\ \mathrm{ln}G_0\ \mathrm{ln}B_0]^T=CCM\cdot[\mathrm{lnR\ ln}G\ \mathrm{ln}B\ \mathrm{ln}N\ 1]^T$
Compound	Transform function	$\mathrm{y}=\alpha\cdot\beta_1^{x_1}\cdot\beta_2^{x_2}$
	Quasi-linearized form	$[\mathrm{lnR}_0\ \mathrm{ln}G_0\ \mathrm{ln}B_0]^T=CCM\cdot[\mathrm{R}\ G\ B\ N\ 1]^T$
S	Transform function	$\mathrm{y}=\exp(\alpha+\frac{\beta_1}{x_1}+\frac{\beta_2}{x_2})$
	Quasi-linearized form	$[\mathrm{lnR}_0\ \mathrm{ln}G_0\ \mathrm{ln}B_0]^T=CCM\cdot\left[\frac{1}{R}\ \frac{1}{G}\ \frac{1}{B}\ \frac{1}{N}\ 1\right]^T$
Cubic B Spline	Transform function	$\mathrm{y}=\alpha+\sum_{j=1}^{2}\sum_{l=0}^{M_j+2}\beta_{j,l}\Omega_3(\frac{x_j-\xi_{j,l-1}}{h_j})$
	Quasi-linearized form	$[\mathrm{R}_0\ G_0\ B_0]^T=CCM\cdot[\Omega_3(\frac{\mathrm{R}-\xi_0}{h})\ldots\Omega_3(\frac{\mathrm{R}-\xi_M}{h})\ \Omega_3(\frac{G-\xi_0}{h})\ldots\Omega_3(\frac{G-\xi_M}{h})\ \Omega_3(\frac{\mathrm{B}-\xi_0}{h})\ldots\Omega_3(\frac{B-\xi_M}{h})\ \Omega_3(\frac{N-\xi_0}{h})\ldots\Omega_3(\frac{N-\xi_M}{h})]^T$
Gaussian Core	Transform function	$\mathrm{y}=\alpha+\sum_{j=1}^{2}\sum_{l=0}^{M_j+2}\beta_{j,l}\,\mathrm{Gau}(\frac{x_j-\xi_{j,l-1}}{h_j})$
	Quasi-linearized form	$[\mathrm{R}_0\ G_0\ B_0]^T=CCM\cdot[\mathrm{Gau}(\frac{\mathrm{R}-\xi_0}{h})\ldots Gau(\frac{\mathrm{R}-\xi_M}{h})Gau(\frac{G-\xi_0}{h})\ldots\mathrm{Gau}(\frac{G-\xi_M}{h})\ \mathrm{Gau}(\frac{\mathrm{B}-\xi_0}{h})\ldots\mathrm{Gau}(\frac{B-\xi_M}{h})Gau(\frac{N-\xi_0}{h})\ldots\mathrm{Gau}(\frac{N-\xi_M}{h})]^T$

form:

$$h(\mathrm{y})=c_0(b_0)+c_1(b_1)\cdot g_1(\mathrm{X})+\cdots+c_p(b_p)\cdot g_p(\mathrm{X}) \quad (7)$$

Here, $h(\mathrm{y})$ represents the function y, $c_i(b_i)(\mathrm{i}=0,1,\ldots,\mathrm{p})$ represents the function b_i, where b_i is a model parameter, and $\mathrm{g}_i(\mathrm{x})(\mathrm{i}=0,1,\ldots,\mathrm{p})$ represents function x. Let $\eta=h(\mathrm{y})$, $\beta_i=\mathrm{c}_i(b_i)$, and $z_i=g_i(\mathrm{x})$. Then,

$$\eta=\beta_0+\beta_1\cdot z_1+\beta_2\cdot z_2+\cdots+\beta_p\cdot z_p \quad (8)$$

This enables linear regression methods to be used.

The details of the quasi-linearization of the nonlinear transfer models are shown in Appendix.

4) MULTICOLLINEARITY IN RGBN CAMERA CHANNELS

Multicollinearity is a common problem in camera color correction applications. It is even more apparent in RGBN camera color correction. Strong correlation between RGBN camera channels decreases the color correction accuracy and robustness when a CCM calculated by OLSR is used. The degree of correction between channels depends on the degree

TABLE 2. RGBN channel correlation coefficients.

Channels	R	G	B	N
R	1	0.8504	0.8137	0.9836
G	0.8504	1	0.9135	0.8560
B	0.8137	0.9135	1	0.8562
N	0.9836	0.8560	0.8562	1

of overlap between each filter's spectral transmittance distribution curve. There exists a strong overlap between R, G, B, and N channels, especially in the NIR band, as shown in Figure 4. Table 2 shows the correlation coefficients of R, G, B, and N channels of an RGBN camera that was used to capture a color checker scene. The four channels are strongly correlated.

A stronger correlation between channels degrades the color correction performance of a CCM calculated by OLSR. Let β_{OLSR} be the regression coefficient of OLSR. Then,

$$\beta_{OLSR} = (\mathrm{P}^T\mathrm{P})^{-1}P^T Q \tag{9}$$

If there exists a completely linear relationship between channels, then $\mathrm{P}^T\mathrm{P}$ is irreversible, and β_{OLSR} cannot be estimated. If there exists a strong correlation between channels, $\det(\mathrm{P}^T\mathrm{P})$ will tend to zero and $(\mathrm{P}^T\mathrm{P})^{-1}$ has a large rounding error. Hence, the color correction results could be unstable.

Biased estimation methods can be used instead of OLSR. On the one hand, $\mathrm{P}^T\mathrm{P}$ is guaranteed to be reversible (e.g. in RLSR). On the other hand, applying the transform and truncation to the data of P could weaken the multicollinearity (e.g., as in PCR and PLSR).

- RLSR

Let β_{Ridge} be the regression coefficient of RLSR. Then [17],

$$\beta_{Ridge} = (\mathrm{P}^T\mathrm{P} + \lambda I)^{-1}P^T Q \tag{10}$$

where λ is a constant number and I is the unit matrix.

Because the L2 norm penalty term is introduced [17], $\mathrm{P}^T\mathrm{P} + \lambda I$ is guaranteed to be reversible. Although OLSR is the optimal unbiased estimation whereas RLSR is a biased estimation, a small-variance biased estimation may perform better than unbiased estimation in color correction. The values of λ are sampled 200 times in $[10^{-5}, 10^{2}]$ with equal distance and determined by 10-fold-cross-validation [18] in this study.

- PCR

Principal component analysis (PCA) [19] is applied to P to obtain k principal components F. Let $\mathrm{F_i}$ be the ith component. Then,

$$\mathrm{F}_i = Pa_i, \quad \|a_i\| = 1 \tag{11}$$

where a_i is the eigenvector the ith biggest eigenvalue of $P^T P/n$. Then, we use OLSR to estimate regression coefficient β_{PCR} of F and Q, calculated as

$$\beta_{PCR} = (\mathrm{F}^T\mathrm{F})^{-1}F^T Q \tag{12}$$

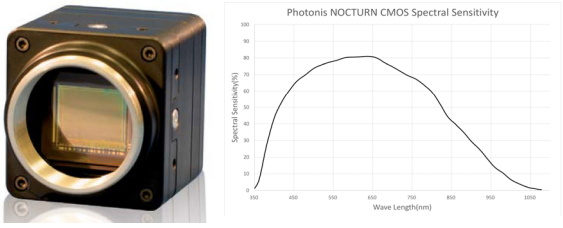

FIGURE 3. (a) Photonis NOCTURN night vision CMOS camera and (b) its spectral sensitivity.

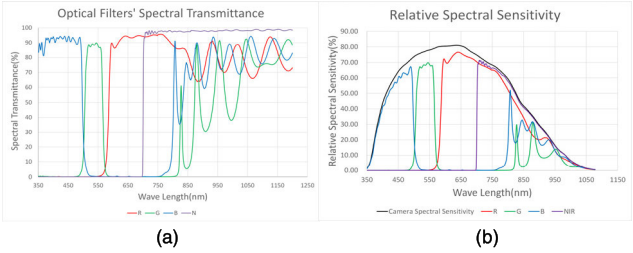

FIGURE 4. (a) Spectral transmittances and (b) relative spectral sensitivities of the RGBN optical filters.

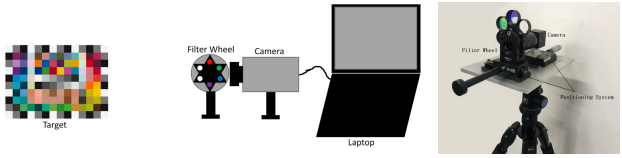

FIGURE 5. Experimental setup.

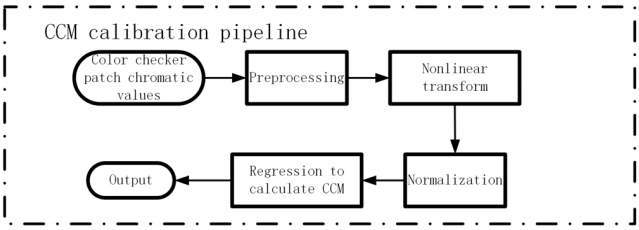

FIGURE 6. RGBN camera CCM calibration pipeline.

- PLSR

Different from PCR, PLSR [20] not only requires the components with the most data information (i.e., $Var(\mathrm{F}_i) \rightarrow \max$), but also requires the independent variable that can best explain the dependent variable (i.e., $r(\mathrm{F}_i, \mathrm{G}_i) \rightarrow \max$). Hence,

$$\begin{aligned} &F_i = Pa_i, \|a_i\| = 1, Var(F_i) \rightarrow \max \\ &G_i = Qc_i, \|c_i\| = 1, Var(G_i) \rightarrow \max \\ &r(F_i, G_i) \rightarrow \max \end{aligned} \tag{13}$$

Regression coefficient β_{PLSR} is calculated using SIMPLS [20] in this study.

B. EXPERIMENTAL SETUP

We used a Photonis NOCTURN XL night vision CMOS grayscale camera as the experimental imaging device (as shown in Figure 3, resolution 1280×1024 pixels, pixel

Algorithm 1 CCM Calibration

Input variables:
P: n ×4 color checker patch chromatic value matrix captured by RGBN camera.
Q: n ×3 ground truth chromatic value matrix
nonLinearMethod: specific nonlinear transform method (chosen in table 1)
regressionMethod: specific regression method (chosen in OLSR,RLSR,PCR,PLSR)
Output variable:
CCM: the color correction matrix

1. normP = P/max(P); % normalize P
2. normQ = Q/max(Q); % normalize Q
3. wbP = whiteBalance(normP); % white balance
4. wbQ = whiteBalance(normQ);
5. transP, transQ = nonLinearTransfer(wbP, wbQ, nonLinearMethod);
% specific nonlinear transform on wbP,wbQ
% some nonlinear transform apply identical transform on variables, such as wbQ in polynomial transform, i.e., transP == wbQ.
6. Q0 = transQ-mean(transQ); % centralize transQ
7. P0 = (transP-mean(transP))/std(transP); % normlize trans P
8. Q1 = shuffle(Q0); % shuffle Q0
9. P1 = shuffle(P0); % shuffle P0 with same seed
10. CCM = tenFoldCrossValidation(P1,Q1, regressionMethod);
% for OLSR, choose CCM with smallest MSE
% for RLSR, choose λ with smallest MSE
% for PCR and PLSR, go through the component numbers from 1, when ΔMSE< ε stop
11. α = mean(transQ)/mean(transP);
% save mean value ratio of transP and transQ for the color correction procedure
% small variance for same illumination
Return CCM

size = 9.7 μm, dynamic range 60 dB, frame rate 100 Hz). An Edmund TECHSPEC 50 mm Vis-NIR fixed-focus lens with a high transmittance in the NIR band was used as the experimental objective lens. Thorlabs FD1D RGBN optical filters that are designed for capturing high contrast ratio color images were used as the experimental optical filters. The R, G, and B channels also have a high transmittance in the NIR band as well as their own bands. A 700 nm high-pass filter was used to capture the N channel. The spectral transmittance curve and the relative spectral sensitivity curve are shown in Figure 4. Finally, the XRITE Color Checker Digital SG 140 was used for color calibration. The overall experimental system is shown in Figure 5.

C. RGBN CAMERA CCM CALIBRATION PIPELINE

The proposed RGBN camera CCM calibration pipeline is shown in Figure 6, and its pseudo code is shown in Algorithm 1. Image preprocessing, which consists of image normalization and white balance adjustment, are first performed on the color checker scene captured by the RGBN camera. Then, a candidate nonlinear transform (chosen from Table 1) is applied on each color patch vector of the color checker image. After a quasi-linearized procedure, the nonlinear feature vectors are converted to high-dimensional feature vectors that can be calculated by linear regression methods. The feature vectors are normalized and the CCM is calculated using a candidate regression method. The CCM is then used in the color correction procedure.

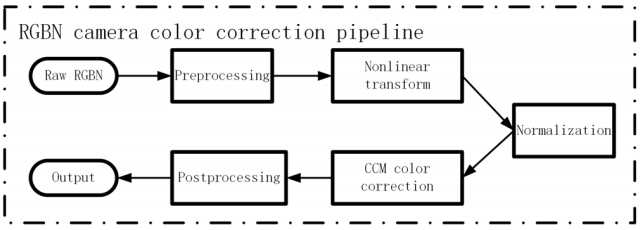

FIGURE 7. RGBN camera color correction pipeline.

Algorithm 2 RGBN Camera Color Correction

Input variables:
P: r ×c ×4 RGBN camera image, where r and c represent image row and column counts, respectively.
CCM: p ×p matrix, CCM calculated in Algorithm 1.
nonLinearMethod: the same nonlinear transform as Algorithm 1
Output variable:
sP: image after color correction

1. normP = P/max(P); % normalization
2. wbP = whiteBalance(normP); % white balance
3. transP = nonLinearTransfer(wbP, nonLinearMethod);
% the same nonlieanr transform as Algorithm 1
4. P0 = (transP-mean(transP))/std(transP); % normalize P
5. reshapeP0 = reshape(P0); % reshape
6. P1 = reshapeP0×hap; % color correction
7. reshapeP1 = reshape(P1); % reshape
8. correctP = reshapeP1+α× mean(transP);
% treat α× mean(transP) as predict image mean value
%α from Algorithm 1
9. sP = gammaCorrection(correctP); % gamma correction
Return sP

D. RGBN CAMERA COLOR CORRECTION PIPELINE

The proposed RGBN camera color correction pipeline is shown in Figure 7. First, image preprocessing (normalization and white balance adjustment) are applied on the images captured by the RGBN camera. Then, a nonlinear transform (as in the CCM calibration) is applied to obtain multi-dimensional feature images. After CCM color correction, the gamma is corrected.

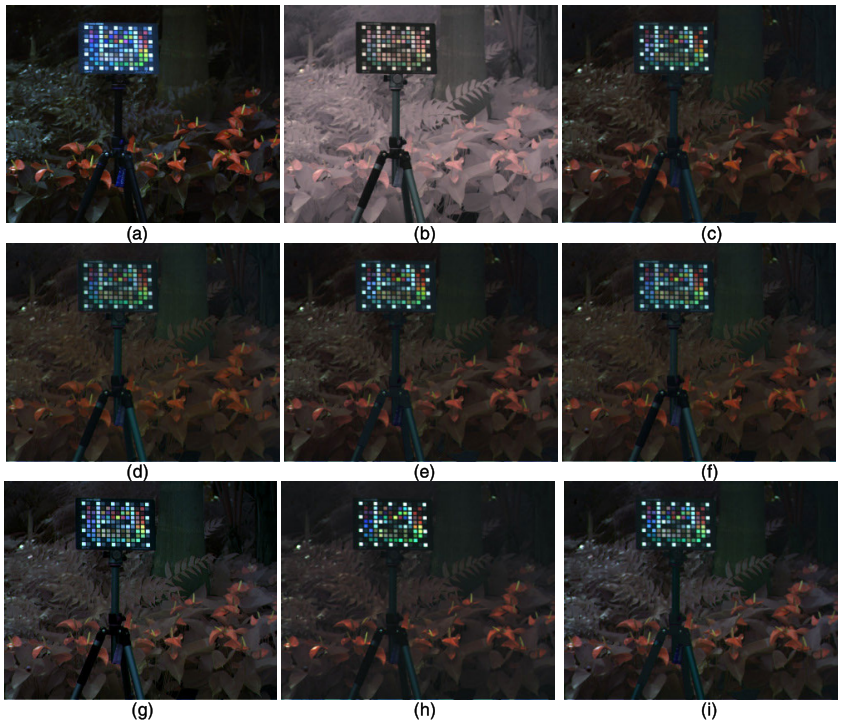

FIGURE 8. RGBN color correction results for scene 1, which consists of plants with a color checker. (a) Image with IRCF, (b) IRCF removal, (c) CZY [1], (d) direct OSLR [5], (e) direct polynomial [5], (f) direct root polynomial [5], (g) PLSR root polynomial, (h) linear compound, and (i) PLSR Gaussian core.

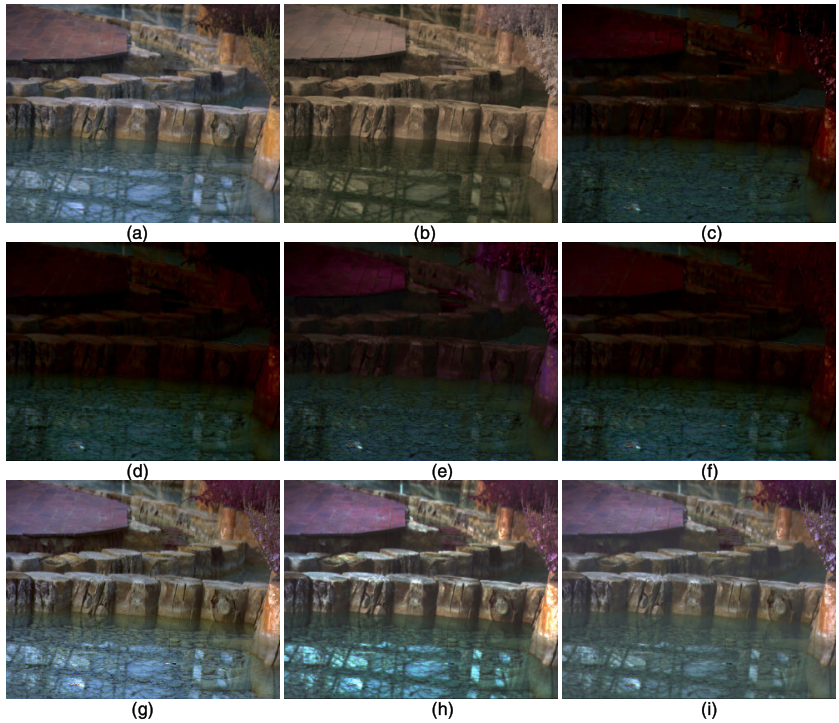

FIGURE 9. RGBN color correction results for scene 2, which consists of plants, wood, and water. (a) Image with IRCF, (b) IRCF removal, (c), CZY, (d) direct OSLR, (e) direct polynomial, (f) direct root polynomial, (g) PLSR root polynomial, (h) linear compound, and (i) PLSR Gaussian core.

III. RESULTS

The CCMs were calibrated with combinations of four regression methods and nine nonlinear transforms using Algorithm 1. Including the combinations for four comparison algorithms and the OLSR method, the total number of CCMs was 41. Then, color correction (Algorithm 2) was performed

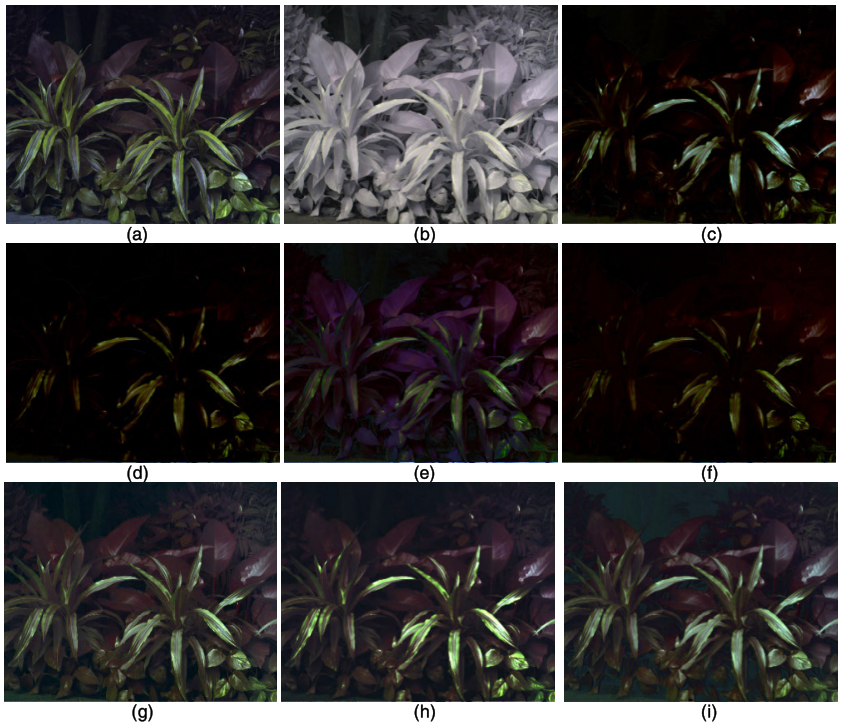

FIGURE 10. RGBN color correction results for scene 3, which consists of plant leaves with different colors. (a) Image with IRCF, (b) IRCF removal, (c) CZY, (d) direct OSLR, (e) direct polynomial, (f) direct root polynomial, (g) PLSR root polynomial, (h) linear compound, and (i) PLSR Gaussian core.

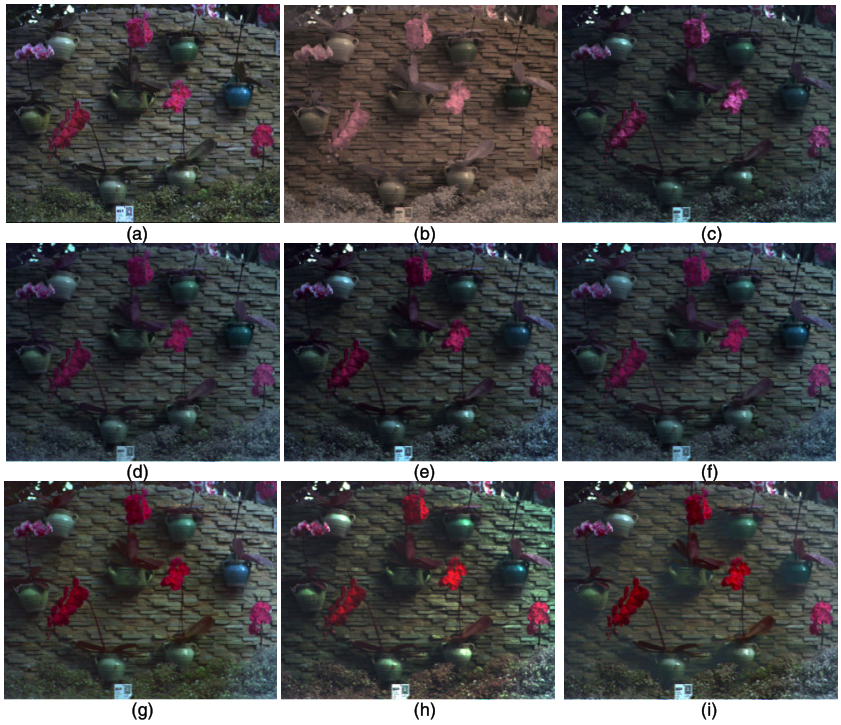

FIGURE 11. RGBN color correction results for scene 4, which consists of flowers, a wall, and stone. (a) Image with IRCF, (b) IRCF removal, (c) CZY, (d) direct OSLR, (e) direct polynomial, (f) direct root polynomial, (g) PLSR root polynomial, (h) linear compound, and (i) PLSR Gaussian core.

with the 41 CCMs. Ten sets of different scenes (a total of 50 images) were tested. Part of the color correction results are shown in Figures 8 to 12.

To evaluate the results, we adopted angular error (AE), CIE 1976 L*a*b* color space color error (ΔE_{ab}), peak SNR (PSNR), and the structural similarity index

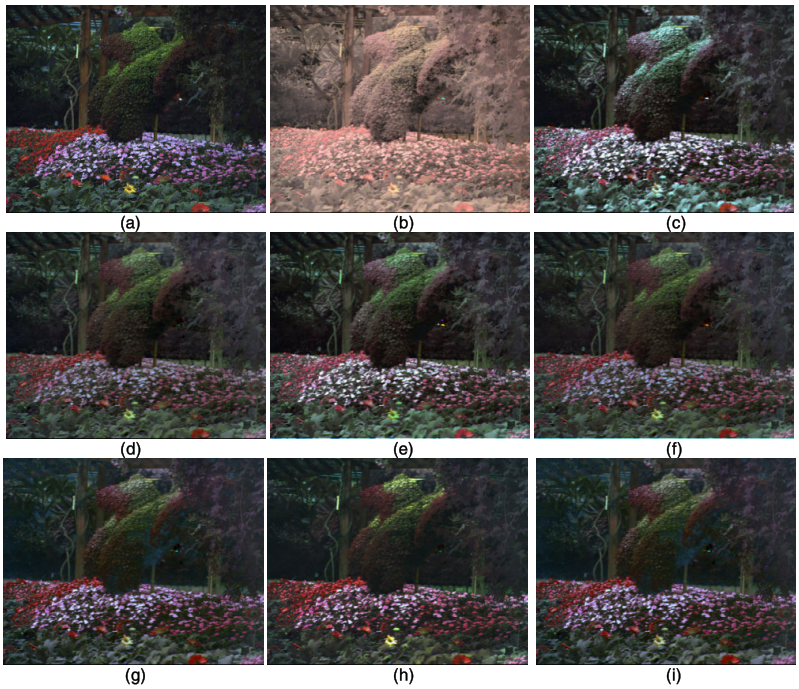

FIGURE 12. RGBN color correction results for scene 5, which consists of flowers with different colors. (a) Image with IRCF, (b) IRCF removal, (c) CZY, (d) direct OSLR, (e) direct polynomial, (f) direct root polynomial, (g) PLSR root polynomial, (h) linear compound, and (i) PLSR Gaussian core.

measure (SSIM). These metrics are described in detail below.

A. AE

AE is used to assess the angular bias between two color vectors. A smaller value of AE indicates that two color vectors are more similar. The equation of AE is

$$\mathrm{AE} = \arccos\left(\frac{XY}{|X|\,|Y|}\right) \tag{14}$$

Here, X is the reference color vector and Y is the evaluated color vector.

B. CIE 1976 L*a*b* COLOR SPACE COLOR ERROR (ΔE_{ab})

CIE1976 L*a*b* color space is a uniform color space that is a nonlinear transformation of the CIE XYZ color space. It is usually used to assess color changes perceived by human vision. Smaller values of ΔE_{ab} are better. Its equation is [21]

$$\begin{aligned}
\Delta E_{ab} &= \sqrt{(\Delta L^*)^2 + (\Delta a^*)^2 + (\Delta b^*)^2} \\
&\begin{cases}
L^* = 116\, f\left(\frac{Y}{Y_n}\right) - 16 \\
a^* = 500\,[f\left(\frac{X}{X_n}\right) - f\left(\frac{Y}{Y_n}\right)] \\
b^* = 200\,[f\left(\frac{Y}{Y_n}\right) - f\left(\frac{Z}{Z_n}\right)]
\end{cases} \\
f(T) &= \begin{cases}
(T)^{\frac{1}{3}} & T > 0.008856 \\
7.787(T) + \dfrac{16}{116} & T \le 0.008856
\end{cases} \\
T &\in \left\{\frac{X}{X_n}, \frac{Y}{Y_n}, \frac{Z}{Z_n}\right\}
\end{aligned} \tag{15}$$

C. PSNR

A bigger PSNR value means the image is more similar to the ground truth. The equation of PSNR is [22]

$$\begin{cases}
PSNR(\mathrm{f}, \mathrm{g}) = 10 \log_{10}\left(\dfrac{(2^{bit} - 1)^2}{MSE(\mathrm{f}, \mathrm{g})}\right) \\
MSE(\mathrm{f}, \mathrm{g}) = \dfrac{1}{MN} \displaystyle\sum_{i=1}^{M} \sum_{j=1}^{N} (\mathrm{f}_{ij} - \mathrm{g}_{ij})^2
\end{cases} \tag{16}$$

Here, f is the reference image, g is the test image, and "bit" is the image's bit depth.

D. SSIM

The range of SSIM is (0,1). A bigger SSIM value means the image is more similar to the ground truth. The equation of SSIM is [23]

$$\begin{cases}
SSIM(f, g) = l(f, g)c(f, g)s(f, g) \\
l(f, g) = \dfrac{2\mu_f \mu_g + C_1}{\mu_f^2 + \mu_g^2 + C_1} \\
c(f, g) = \dfrac{2\sigma_f \sigma_g + C_2}{\sigma_f^2 + \sigma_g^2 + C_2} \\
s(f, g) = \dfrac{\sigma_{fg} + C_3}{\sigma_f \sigma_g + C_3}
\end{cases} \tag{17}$$

Here, μ_f and μ_g are the mean values of the whole images f and g, respectively, and σ_f and σ_g are their standard deviations. In addition, σ_{fg} is the covariance of images f and g and C_1, C_2, and C_3 are constants to avoid division by zero.

The results for 10 sets of test scene are shown in Table 3. The results for the PCR- and PLSR-based logarithm, inverse,

TABLE 3. Evaluation indices of different color correction methods.

Index	AE (°)			ΔE_{ab}			PSNR			SSIM ($\times 10^{-2}$)		
	mean	max	std	mean	max	std	mean	max	std	mean	max	std
Input	12.38	18.40	4.38	23.88	37.13	8.92	13.65	19.95	3.72	73.06	94.80	12.47
CZY	16.18	37.68	11.83	12.76	30.25	7.02	19.34	25.20	3.86	83.56	97.32	17.72
Direct OLSR	18.65	40.92	13.31	13.64	31.59	7.16	18.84	23.69	3.82	80.11	96.57	21.01
Direct polynomial	11.23	25.52	6.13	12.49	29.36	6.97	19.91	25.90	3.83	88.97	97.27	12.00
Direct root polynomial	20.84	48.07	11.83	13.58	31.47	7.19	18.80	24.20	3.86	81.24	96.63	19.74
OLSR	10.32	17.42	4.20	10.46	20.46	4.26	20.46	26.63	3.56	95.60	**98.89**	2.58
OLSR+ Polynomial	9.90	19.42	4.47	10.54	19.24	4.11	21.99	27.67	3.16	94.84	98.48	3.30
OLSR+ Root polynomial	10.65	17.18	3.99	10.78	21.02	4.47	22.08	27.17	3.20	95.43	98.56	2.22
OLSR+ Logarithm	10.21	17.56	3.38	12.10	19.68	4.01	20.46	24.32	2.90	93.88	97.09	3.40
OLSR+ Inverse	16.24	22.72	6.83	27.67	45.77	10.00	12.87	19.11	3.39	77.79	94.44	9.92
OLSR+ Power	6.98	10.25	1.96	10.94	18.26	4.71	20.45	24.32	2.90	95.25	98.06	3.08
OLSR+ Compound	**6.51**	**9.70**	**1.87**	**9.83**	**17.07**	4.06	21.98	**28.38**	3.30	**96.34**	98.44	**1.91**
OLSR+ S	16.87	26.92	7.55	29.90	50.55	11.69	11.37	18.94	4.07	75.19	94.61	12.10
OLSR+ Cubic B spline	18.82	39.04	9.26	54.79	75.96	10.95	7.74	13.25	3.72	47.50	76.46	19.83
OLSR+ Gaussian core	14.90	26.51	7.76	14.21	27.97	7.27	20.30	27.36	3.84	91.78	97.75	5.65
RLSR+ Cubic B spline	13.50	25.09	5.66	12.57	19.25	4.57	20.55	27.36	4.11	92.72	98.68	3.88
RLSR+ Gaussian core	14.89	26.49	7.76	14.20	27.96	7.27	20.30	27.36	3.84	91.78	97.75	5.65
PCR+ Polynomial	9.32	17.11	3.94	10.51	18.38	3.94	22.08	27.64	3.07	95.11	98.49	2.89
PCR+ Root polynomial	10.38	16.96	3.95	10.64	20.12	4.25	22.02	26.90	3.16	95.45	98.54	2.24
PCR+ Cubic B spline	11.60	17.65	4.17	11.21	18.46	4.26	20.64	27.27	3.55	94.11	98.73	3.57
PCR+ Gaussian core	9.86	17.78	4.33	10.41	19.39	3.98	22.37	27.82	3.36	95.33	98.45	2.41
PLSR+ Polynomial	9.41	17.90	4.08	10.47	18.72	4.01	22.06	27.73	3.15	95.06	98.49	3.05
PLSR+ Root polynomial	10.57	17.54	4.07	10.76	20.86	4.43	22.07	26.97	3.18	95.46	98.55	2.26
PLSR+ Cubic B spline	11.76	18.68	4.21	11.33	18.68	4.28	20.65	27.26	3.58	94.06	98.73	3.59
PLSR+ Gaussian core	9.34	17.37	4.30	10.36	18.95	**3.92**	**22.43**	27.96	**2.89**	95.23	98.28	2.64

power, compound, and S transforms have the same number of components as OLSR after 10-fold cross-validation. Hence, the values of the final evaluation indices are the same as those of OLSR and they are omitted. RLSR based polynomial, root

polynomial, logarithm, inverse, power, compound, S methods obtain a λ of less than 10^{-2}. The variation in the evaluation are so small, they are also omitted. A comparison shows that the OLSR-based compound and PLSR-based Gaussian core combinations yield the best performance.

The OLSR-, RLSR-, PCR-, and PLSR-based compound RGBN camera color correction methods yield similar results. For the compound transform, PCR and PLSR return a component count that is equal to the total component count through 10-fold cross-validation. Hence, PCR- and PLSR-based compound methods are equal to the OLSR-based compound in this case. The RLSR-based compound obtains a λ that is too small to improve the results and perform similarly. The OLSR-based compound method is recommended because, of the four regression methods, OLSR is the easiest to calculate. Applying the compound transform to the image has the same effect as some preprocessing procedures in color image applications. The compound transform applies a logarithm transform to dependent variables and then fits them with the independent variables. Logarithm transform preprocessing has been adopted in color correction and color transfer applications and is thought to have a basis in human visual physiology [24]. The relationship between the compound transform and image preprocessing techniques remains a task for further study.

The Gaussian core transform and cubic B spline transform are typical nonlinear transform models in regression methods. If there is plenty of sample data, these models have a better capacity to express more complicated relationships than nonlinear transform models based on a single type of function. However, only 96 reference color patches are used in CCM calibration. Hence, the PLSR method is adopted to select the components that best express the model. This is a tradeoff between the expressiveness of the model and the risk of overfitting. The results in Table 3 show that the Gaussian core transform outperforms the cubic B spline transform and is more robust. The Gaussian core transform has a uniform function form in its domain $(-\infty, +\infty)$. When applying the Gaussian core transform to an image, each channel interval's feature takes all intervals into consideration. When applying the cubic B spline transform, each channel interval's feature only takes its neighborhood into consideration. Hence, it is more difficult to balance model expressiveness and overfitting risk in the cubic B spline transform given limited data.

In summary, the OLSR-based compound and PLSR-based Gaussian core methods have the best performance for RGBN camera color-correction applications.

IV. CONCLUSION

RGBN cameras can capture visible and NIR information simultaneously, but introduce color desaturation into the images. The image color bias becomes obvious especially when capturing outdoor scenes with strong NIR illumination. The inclusion of NIR light makes the relationship between the color biased image and the ground truth image more complicated. Moreover, the multicollinearity in RGBN camera channels makes the OLSR color correction result unsatisfactory. Hence, in this study, the combination of four regression methods and nine nonlinear transform color correction methods were investigated and compared in a uniform color correction pipeline. The OLSR-based compound and PLSR-based Gaussian core methods achieve the best color correction accuracy and are the most robust. These results demonstrate that the proposed RGBN camera color correction pipeline performs better than the traditional OLSR method. However, the proposed RGBN camera color correction method still needs a pre-calibrated CCM, as in traditional CCM color correction methods. In future work, to obtain more accurate color correction results and high SNR images, we would like to modify the spectral transmittance of the optical filters and further study color correction in low-light multi-spectral imaging devices.

APPENDIX
QUASI-LINEARIZATION OF THE NONLINEAR TRANSFORM

A. POLYNOMIAL MODEL

For the polynomial model,

$\mathrm{y} = \alpha + \beta_1 \cdot x_1 + \beta_2 \cdot x_2 + \beta_3 \cdot x_1^2 + \beta_4 \cdot x_2^2 + \beta_5 \cdot x_1 \cdot x_2$. Let $\eta = y, \mathrm{z}_1 = x_1, \mathrm{z}_2 = x_2, \mathrm{z}_3 = x_1^2, \mathrm{z}_4 = x_2^2, \mathrm{z}_5 = x_1 x_2$. Then,

$$\eta = \alpha + \beta_1 \cdot z_1 + \beta_2 \cdot z_2 + \beta_3 \cdot z_3 + \beta_4 \cdot z_4 + \beta_5 \cdot z_5. \quad (18)$$

B. ROOT POLYNOMIAL MODEL

For the root polynomial model,

$$\mathrm{y} = \alpha + \beta_1 \cdot x_1 + \beta_2 \cdot x_2 + \beta_3 \cdot \sqrt{x_1 \cdot x_2}.$$

Let $\eta = y, \mathrm{z}_1 = x_1, \mathrm{z}_2 = x_2, \mathrm{z}_3 = \sqrt{x_1 \cdot x_2}$. Then,

$$\eta = \alpha + \beta_1 \cdot z_1 + \beta_2 \cdot z_2 + \beta_3 \cdot z_3. \quad (19)$$

C. LOGARITHM MODEL

For the logarithm model $\mathrm{y} = \alpha + \beta_1 \cdot \ln x_1 + \beta_2 \cdot \ln x_2$.

Let $\eta = y, \mathrm{Z}_i = x_i (i = 1, 2)$. Then,

$$\eta = \alpha + \beta_1 \cdot z_1 + \beta_2 \cdot z_2. \quad (20)$$

D. INVERSE MODEL

For the inverse model, $\mathrm{y} = \alpha + \frac{\beta_1}{x_1} + \frac{\beta_2}{x_2}$.

Let $\eta = y, \mathrm{Z}_i = \frac{1}{x_i}$. Then,

$$\eta = \alpha + \beta_1 \cdot z_1 + \beta_2 \cdot z_2. \quad (21)$$

E. POWER MODEL

For the power model, $y = \alpha \cdot x_1^{\beta_1} \cdot x_2^{\beta_2}$ and $\ln y = \ln \alpha + x_1 \ln \beta_1 + x_2 \ln \beta_2$. Let $\eta = \ln y$, $\gamma = \ln \alpha$, and $\mathrm{z}_i = \ln x_i (i = 1, 2)$. Then,

$$\eta = \gamma + \beta_1 \cdot z_1 + \beta_2 \cdot z_2. \quad (22)$$

F. COMPOUND MODEL

For the compound model, $y = \alpha \cdot \beta_1^{x_1} \cdot \beta_2^{x_2}$ and $\ln y = \ln \alpha + x_1 \ln \beta_1 + x_2 \ln \beta_2$. Let $\eta = \ln y, \mathrm{z}_i = x_i, \lambda_i = \ln \beta_i \ \ (i = 1, 2)$. Then,

$$\eta = \alpha + \lambda_1 \cdot z_1 + \lambda_2 \cdot z_2. \quad (23)$$

G. S MODEL

For the S model, $y = \exp(\alpha + \frac{\beta_1}{x_1} + \frac{\beta_2}{x_2})$ and $\ln y = \alpha + \frac{\beta_1}{x_1} + \frac{\beta_2}{x_2}$.

Let $\eta = \ln y$, $z_i = \frac{1}{x_i}(i = 1, 2)$. Then,

$$\eta = \alpha + \beta_1 \cdot z_1 + \beta_2 \cdot z_2. \tag{24}$$

H. CUBIC B SPLINE MODEL

1) Let $x_i(i \in [R, G, B, N])$ be the input image channel. Divide x_i into M intervals so that there are M+1 interval endpoints. Let ξ_i be the endpoints of channel i; then $\xi_i = [\xi_0, \ldots, \xi_M]$. In addition, the interval length $h_i = \frac{\max(x_i) - \min(x_i)}{M}$. In this paper, M = 5. For example, if the maximum pixel value of the red channel max(R) = 1, and the minimum value min(R) = 0, then $\xi_R = [0, 0.2, 0.4, 0.6, 0.8, 1]$ and $h_R = 0.2$.
2) All x_i are cubic-B-spline transformed in each interval. We then obtain new feature vectors $z_{i,j} = \Omega_3(\frac{x_j - \xi_{i,j}}{h_i})$. Moreover,

$$\begin{aligned}\Omega_3(x) &= \frac{1}{6}(x+2)_+^3 - \frac{2}{3}(x+1)_+^3 \\ &\quad + x_+^3 - \frac{2}{3}(x-1)_+^3 + \frac{1}{6}(x-2)_+^3 \\ (x-a)_+^3 &= \begin{cases}(x-a)^3 & (x \geq a) \\ 0 & (x < a)\end{cases}\end{aligned} \tag{25}$$

3) The normalized feature vectors can be used in regression methods, e.g.,

$$\begin{aligned}[R_0 G_0 B_0]^T = CCM \cdot [&\Omega_3(\frac{R-\xi_0}{h}) \ldots \Omega_3(\frac{R-\xi_M}{h}) \\ &\Omega_3(\frac{G-\xi_0}{h}) \ldots \Omega_3(\frac{G-\xi_M}{h}) \\ &\Omega_3(\frac{B-\xi_0}{h}) \ldots \Omega_3(\frac{B-\xi_M}{h}) \\ &\Omega_3(\frac{N-\xi_0}{h}) \ldots \Omega_3(\frac{N-\xi_M}{h})]^T.\end{aligned} \tag{26}$$

I. GAUSSIAN CORE MODEL

1) Let $x_i(i \in [R, G, B, N])$ be the input image channel. Divide x_i into M intervals so that there are M+1 interval endpoints. Let ξ_i be the endpoints of channel i; then $\xi_i = [\xi_0, \ldots, \xi_M]$. Moreover, the interval length $h_i = \frac{\max(x_i) - \min(x_i)}{M}$.
2) All x_i are Gaussian-core transformed in each interval to obtain feature vectors $z_{i,j} = \mathrm{Gau}(\frac{x_j - \xi_{i,j}}{h_i})$. Moreover,

$$Gau(x) = \frac{1}{\sqrt{2\pi}} \exp(-\frac{x^2}{2}) \quad (-\infty < x < \infty). \tag{27}$$

3) The normalized feature vectors can be used in regression methods, e.g.,

$$\begin{aligned}[R_0\ G_0\ B_0]^T = CCM \cdot [&\mathrm{Gau}(\frac{R-\xi_0}{h}) \ldots Gau(\frac{R-\xi_M}{h}) \\ &Gau(\frac{G-\xi_0}{h}) \ldots Gau(\frac{G-\xi_M}{h}) \\ &Gau(\frac{B-\xi_0}{h}) \ldots Gau(\frac{B-\xi_M}{h}) \\ &Gau(\frac{N-\xi_0}{h}) \ldots \mathrm{Gau}(\frac{N-\xi_M}{h})]^T.\end{aligned} \tag{28}$$

REFERENCES

[1] Z. Chen, X. Wang, and R. Liang, "RGB-NIR multispectral camera," *Opt. Express*, vol. 22, no. 5, p. 4985, Mar. 2014.
[2] Z. Sadeghipoor, J.-B. Thomas, and S. Süsstrunk, "Demultiplexing visible and near-infrared information in single-sensor multispectral imaging," in *Proc. Color Imag. Conf.*, vol. 2016, no. 1, Nov. 2016, pp. 76–81.
[3] H. Yamashita, D. Sugimura, and T. Hamamoto, "Enhancing low-light color images using an RGB-NIR single sensor," in *Proc. Vis. Commun. Image Process. (VCIP)*, Dec. 2015, pp. 1–4.
[4] B. K. Park, W. Choe, J. G. Lim, S. D. Lee, and C. Kim, "Color correction with edge preserving and minimal SNR decrease using multi-layer decomposition," *Proc. SPIE*, vol. 8296, Feb. 2012, Art. no. 829613.
[5] Y. Monno, M. Tanaka, and M. Okutomi, "N-to-SRGB mapping for single-sensor multispectral imaging," in *Proc. IEEE Int. Conf. Comput. Vis. Workshop (ICCVW)*, Dec. 2015, pp. 66–73.
[6] H. Teranaka, Y. Monno, M. Tanaka, and M. Ok, "Single-sensor RGB and NIR image acquisition: Toward optimal performance by taking account of CFA pattern, demosaicking, and color correction," *Electron. Imag.*, vol. 2016, no. 18, pp. 1–6, Feb. 2016.
[7] C. H. Park, H. M. Oh, and M. G. Kang, "Color Restoration for Infrared Cutoff Filter Removed RGBN Multispectral Filter Array Image Sensor," in *Proc. 10th Int. Conf. Comput. Vis. Theory Appl.*, 2015, pp. 30–37.
[8] J. Y. Kwon, C. H. Park, and M. G. Kang, "Least square based multi-spectral color interpolation algorithm for RGB-NIR image sensors," in *Proc. 10th Int. Conf. Comput. Vis. Theory Appl.*, 2015, pp. 38–45.
[9] C. Park and M. Kang, "Color restoration of RGBN multispectral filter array sensor images based on spectral decomposition," *Sensors*, vol. 16, no. 5, p. 719, May 2016.
[10] D. Hertel, H. Marechal, D. A. Tefera, W. Fan, and R. Hicks, "A low-cost VIS-NIR true color night vision video system based on a wide dynamic range CMOS imager," in *Proc. IEEE Intell. Vehicles Symp.*, Jun. 2009, pp. 273–278.
[11] D. Sugimura, T. Mikami, H. Yamashita, and T. Hamamoto, "Enhancing color images of extremely low light scenes based on RGB/NIR images acquisition with different exposure times," *IEEE Trans. Image Process.*, vol. 24, no. 11, pp. 3586–3597, Nov. 2015.
[12] H. Yamashita, D. Sugimura, and T. Hamamoto, "Low-light color image enhancement via iterative noise reduction using RGB/NIR sensor," *J. Electron. Imag.*, vol. 26, no. 04, p. 1, Aug. 2017.
[13] C. Aguilera, X. Soria, A. D. Sappa, and R. Toledo, "RGBN multispectral images: A novel color restoration approach," in *Proc. Int. Conf. Practical Appl. Agents Multi-Agent Syst.* Cham, Switzerland: Springer, 2017, pp. 155–163.
[14] X. Soria, A. D. Sappa, and A. Akbarinia, "Multispectral single-sensor RGB-NIR imaging: New challenges and opportunities," in *Proc. 7th Int. Conf. Image Process. Theory, Tools Appl. (IPTA)*, Nov. 2017, pp. 1–6.
[15] X. Soria, A. Sappa, and R. Hammoud, "Wide-band color imagery restoration for RGB-NIR single sensor images," *Sensors*, vol. 18, no. 7, p. 2059, Jun. 2018.
[16] M. Ebner, *Color Constancy*. vol. 7. Hoboken, NJ, USA: Wiley, 2007, pp. 46–63.
[17] D. W. Marquardt and R. D. Snee, "Ridge regression in practice," *Amer. Statistician*, vol. 29, no. 1, pp. 3–20, Feb. 1975.
[18] S. Arlot and A. Celisse, "A survey of CRoss-validation procedures for model selection," *Statist. Surv.*, vol. 4, no. 0, pp. 40–79, 2010.
[19] T. Naes and H. Martens, "Comparison of prediction methods for multicollinear data," *Commun. Stat.-Simul. Comput.*, vol. 14, no. 3, pp. 545–576, Jan. 1985.
[20] S. De Jong, "SIMPLS: An alternative approach to partial least squares regression," *Chemometric Intell. Lab. Syst.*, vol. 18, no. 3, pp. 251–263, Mar. 1993.
[21] N. Liao, J. Shi, and W. Wu, *An Introduction to Digital Color Management System*. Beijing, China: Beijing Institute of Technology Press, 2009, pp. 46–47.
[22] A. Hore and D. Ziou, "Image quality metrics: PSNR vs. SSIM," in *Proc. 20th Int. Conf. Pattern Recognit.*, Aug. 2010, pp. 2366–2369.
[23] Z. Wang, E. Simoncelli, and A. Bovik, "Multiscale structural similarity for image quality assessment," in *Proc. 37th Asilomar Conf. Signals, Syst. Comput.*, vol. 2, Jul. 2004, pp. 1398–1402.
[24] E. Reinhard, M. Adhikhmin, B. Gooch, and P. Shirley, "Color transfer between images," *IEEE Comput. Grap. Appl.*, vol. 21, no. 4, pp. 34–41, Jul./Aug. 2001.

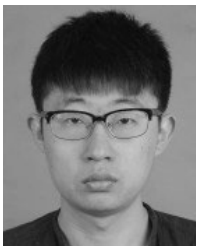

ZHENGHAO HAN received the B.S. degree in electronics science and technology from the Beijing Institute of Technology, Beijing, China, in 2015, where he is currently pursuing the Ph.D. degree with the Key Laboratory of Photoelectronic Imaging Technology and System. His main research interests include low light level color imaging and real-time image processing.

WEIQI JIN received the Ph.D. degree in military optics from the Beijing Institute of Technology, China, in 1990. He has been a Ph.D. Tutor, Professor, and the Director of the Key Laboratory of Optoelectronic Imaging Technology and Systems. He is currently the Director of the Chinese Optical Society and the Beijing Institute of Optics, and an advanced member of the Chinese Institute of Electronics. His main research interests include infrared imaging technology, photoelectric image processing, and photoelectric detection and instrumentation.

LI LI received the B.S., M.S., and Ph.D. degrees in optical engineering from the Beijing Institute of Technology, China, in 2000, 2004, and 2008, respectively. He has been a Lecturer with the Beijing Institute of Technology, Optical Engineering. His main research interests include image and video processing technology, real-time image processing, digital image processing, and imaging systems and technology.

XIA WANG received the Ph.D. degree in automation from the China University of Mining and Technology, in 1999. She is currently an Associate Professor with the Beijing Institute of Technology, where she is currently the Vice Dean of the Institute of Photoelectric Imaging and Information Engineering. Her current research interests are in optoelectronic detection, spectrum analysis, and imaging technology.

XIAOFENG BAI received the Ph.D. degree in optical engineering from the Kunming Institute of Physics, China, in 2019. He has been a Senior Engineer at a level of research worker of the Kunming Institute of Physics, and a Committeeman of the Automatic Measurement and Control Technology Professional Committee of the Chinese Society for Measurement. His main research interests include low-light-level image intensifier technology and optical measurement.

HAILIN WANG received the B.S. degree in optoelectronics information science and engineering from the Beijing Institute of Technology, Beijing, China, in 2018. She is currently pursuing the M.S. degree with the Key Laboratory of Photoelectronic Imaging Technology and System. Her main research interests include low light level color imaging and image processing.